Photovoltaic Effects of Dye-Sensitized Solar Cells Using Double-Layered TiO₂ Photoelectrodes and Pyrazine-Based Photosensitizers

Mi-Ra Kim, Thanh Chung Pham, Hyun-Seock Yang, Sung Heum Park, Seah Yang, Myeongkee Park, Sang Gil Lee, and Songyi Lee*

Read Online

ACCESS | Metrics & More | Article Recommendations | Supporting Information
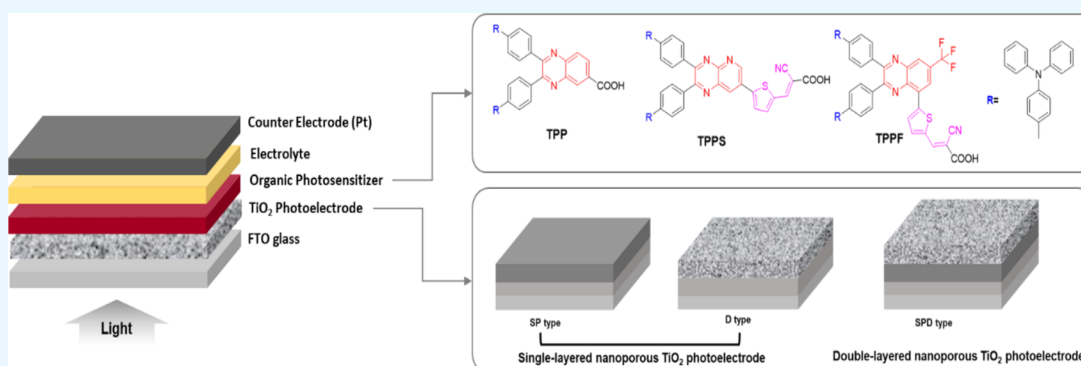
ABSTRACT: In this study, to obtain high performances of the dye-sensitized solar cells using the optimal TiO₂ photoelectrode for the synthesized pyrazine-based organic photosensitizers, three types of TiO₂ photoelectrodes were fabricated and evaluated for comparison. The double-layered nanoporous TiO₂ photoelectrode (SPD type) consisted of a dispersed TiO₂ layer and a transparent TiO₂ layer. The single-layered nanoporous TiO₂ photoelectrodes (D type and SP type) consisted of a dispersed TiO₂ layer and a transparent TiO₂ layer, respectively. The surface area, pore volume, and crystalline structures of the three types of TiO₂ photoelectrodes were analyzed by Brunauer−Emmett−Teller method, field-emission scanning electron microscopy, and X-ray diffractometry to confirm their crystallinity and surface morphology. The structures of the three types of TiO₂ photoelectrode-adsorbed organic sensitizers were investigated using X-ray photoelectron spectroscopy. The photovoltaic performances of DSSC devices using three organic photosensitizers adsorbed onto the three types of TiO₂ photoelectrodes were investigated under a light intensity of 100 mW/cm² at AM 1.5. The DSSC device using double-layered SPD type TiO₂ photoelectrodes displayed 1.31∼2.64% efficiency, compared to single-layered SP type TiO₂ photoelectrodes (1.31∼2.50%) and D type TiO₂ photoelectrodes (0.90∼1.54%), using organic photosensitizers. The DSSC device using the SPD type TiO₂ photoelectrode and trifluoromethylbenzopyrazine (TPPF) as a photosensitizer showed the highest performances: J_{sc} of 5.69 mA/cm², V_{oc} of 0.69 V, FF of 0.67, and efficiency of 2.64%. The relationship between photovoltaic effects and interfacial resistance characteristics of DSSCs using the three organic photosensitizers adsorbed onto the three types of TiO₂ photoelectrodes could be interpreted from interfacial resistances according to frequency through impedance analysis.

INTRODUCTION

Solar energy is one of the cleanest and most abundant renewable resources. To make useful utilization of abundant renewable solar energy, the collection and conversion of solar energy must be highly efficient. In this regard, photovoltaic (PV) plays an important role in harnessing solar energy, which is currently dominated primarily by silicon-based solar cells.

However, the manufacturing of silicon-based solar cells requires high melting temperatures and ultra-pure material, which leads to a complex and expensive manufacturing process.[1] Also, the scarcity of gold or silver, which are the most used electrode materials, greatly limits the establishment of high-power photovoltaic systems in the future. This has

motivated many researchers to develop strategies for solar energy conversion based on commercially available materials that are abundant on Earth, non-toxic, and easy to post-process. In this regard, dye-sensitized solar cells (DSSCs) made of mesoscopic metal oxides (TiO₂, ZnO, SnO₂, and Nb₂O₅) and organic dyes can meet the standards as a suitable
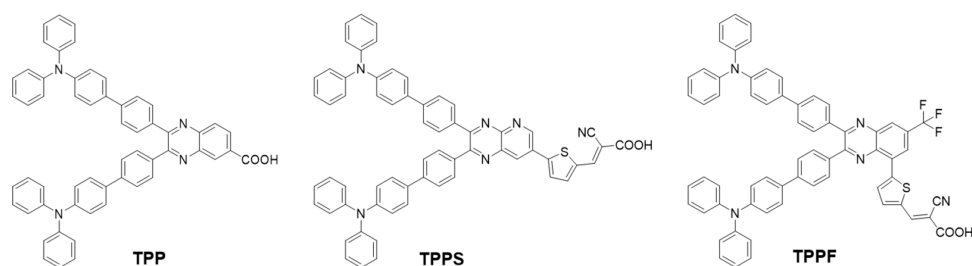
Figure 1. Chemical structures of the three organic photosensitizers (TPP, TPPS, and TPPF).

(a) FTO glass ; (b) Blocking Layer (BL, compact TiO_2) ; (c) TiO_2 Layer (SP, transparent TiO_2) ; (c-1) TiO_2 Layer (D, dispersed TiO_2)
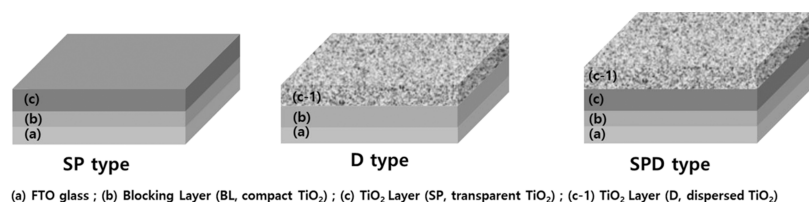
Figure 2. Structures of the three types of TiO_2 photoelectrodes (SP type, D type, and SPD type).

alternative if high efficiency and stability can be realized.[2,3] Metal oxide acts as an electron acceptor and in most cases, it also acts as an electron transporter by adsorbing the dyes.[4,5] Among various metal oxides, mesoscopic titanium dioxide (TiO_2) is the most widely studied so far due to its high chemical stability, low cost, and non-toxicity.[5−8] In addition, it also has a high specific surface area to adsorb dyes and easy band gap control through surface modification. Most metal oxides have more than one crystalline phase. In the case of titanium dioxide, it naturally has three crystalline phases: anatase (tetragonal), rutile (tetragonal), and brookite (orthorhombic). Rutile is thermodynamically the most stable form; however, anatase is the preferred structure in DSSCs because it has a larger band gap (3.2 vs 3.0 eV for rutile) and a higher conduction band edge energy (E_c). This leads to a higher Fermi level and V_{oc} in DSSCs for the same conduction band electron concentration. The anatase phase is preferred in DSSCs because of its high conduction band energy and slow recombination rate of charge carriers.[9−11]

In recent advances in photoelectrodes, nanostructures of TiO_2 to apply on DSSCs can be fabricated using several methods such as hydrothermal synthesis or sol−gel method,[12] spray method,[13] electrospinning method,[14] microwave synthesis,[15] and direct oxidation method.[16]

Several improvements to TiO_2 photoelectrodes have been shown to enhance the overall photovoltaic performances of the DSSCs over many years of development. TiO_2 photoelectrodes were modified and developed through morphology improvements and application of composite/hybrid materials. In a study by Zhang et al., mesoporous TiO_2 microspheres were prepared, and the double-layered DSSC of TiO_2 microspheres as a scattering layer displays 5.61% efficiency, compared to the single TiO_2 microsphere layer (2.14%) and single P25 layer (2.67%)-based DSSC.[17] Chen et al. reported a DSSC with a maximum conversion efficiency of 7.56% achieved with the photoelectrode consisting of a popcorn-like TiO_2 (P−TiO_2) layer.[18] A 3D-TiO_2 nanorod photoelectrode was prepared, and its photovoltaic characteristics were investigated by Khakpour et al.[19] Novel $MoWO_4$ with ZnO nanoflowers was synthesized on multi-walled carbon nanotubes through a simple hydrothermal method, and this unique structure was applied as a counter electrode for DSSCs for the first time.[20] A novel nanocomposite composed of graphene-La_2CrFeW_6 perovskite compounds with an organic−inorganic counter electrode was developed with CdSe, gallic acid, urea, and sulfate in DSSCs by a simple hydrothermal technique.[21]

The significant limiting variable for efficient DSSC is the interfacial recombination rate and interfacial charge resistance. In addition, the slow transportation rate of electrons arising from several trapping/entrapping events arising inside the grain boundaries and low charge transport will result in high recombination at the interface and reduce device performance.

In particular, in case of applying a novel synthesized photosensitizer, it is necessary to study a method that improves the applicability and efficiency of a matched photoelectrode. In this study, three different TiO_2 photoelectrodes were applied to find TiO_2 photoelectrodes suitable for the three synthesized organic photosensitizers. By a solution-processed spin-coating method, well-defined nanostructured TiO_2 photoelectrodes were mainly used in the device with an excellent transmittance, single-crystalline properties, a uniform film thickness, and a large effective area.[22] Although TiO_2 photoelectrodes fabricated by the spin-coating method had many advantages, they were too thin to adsorb a sufficient amount of organic photosensitizers. Therefore, in order to adsorb a sufficient amount of organic photosensitizers in this study, the doctor blade method was applied to fabricate a TiO_2 photoelectrode that was sufficiently thick and had a large specific surface area. The SP type TiO_2 photoelectrode was transparent and had high permeability, while the D type TiO_2 photoelectrode was opaque and showed translucency. In order to increase light retention due to the light scattering effect inside the TiO_2 photoelectrode, the D type over the SP type was introduced and optimized. A DSSC according to each organic photosensitizer and the TiO_2 photoelectrode analyzed the impedance results and photoconversion efficiency, and the photovoltaic effects of the DSSC could be interpreted through the resistance generated at the interface of the DSSC device.

To investigate the photovoltaic effects of DSSCs as crystallographic properties of photoelectrodes suitable for the three synthesized organic photosensitizers (TPP, TPPS, and TPPF, as shown in Figure 1), we prepared three types of nanoporous TiO_2 photoelectrodes: double-layered nanoporous

TiO$_2$ photoelectrode (SPD type) consisting of a dispersed TiO$_2$ layer and a transparent TiO$_2$ layer, single-layered nanoporous TiO$_2$ photoelectrode consisting of a dispersed TiO$_2$ layer (D type), and single-layered nanoporous TiO$_2$ photoelectrode consisting of a transparent TiO$_2$ layer (SP type). The structures of three types of TiO$_2$ photoelectrodes were analyzed by Brunauer–Emmett–Teller (BET), field-emission scanning electron microscopy (FE-SEM), and X-ray diffractometry (XRD), and the structures of the three types of TiO$_2$ photoelectrode-adsorbed organic sensitizers were investigated using X-ray photoelectron spectroscopy (XPS). The three types of TiO$_2$ photoelectrodes were investigated on their surface area, pore volume, and crystalline structure to confirm their crystallinity and surface morphology. All photoelectrodes (SPD, D, and SP type, as shown in Figure 2) were respectively adsorbed by the three synthesized organic photosensitizers and applied to the DSSCs. In a previous study, we developed a series of new organic D−π−A type and D−π−A−π′−A′ type photosensitizers based on pyrazine derivatives (TPP: benzopyrazine; TPPS: pyrido[3,4-b]pyrazine; TPPF: trifluoromethylbenzopyrazine) as acceptors (A), triphenylamine groups as donors(D), and phenyl groups as linkers (π).[23] The thiophene-cyanoacryl group was applied as the auxiliary heterocyclic linker-acceptor (π′−A′). In general, organic photosensitizers have a D−π−A structure that includes an electron donor (D), a π-conjugated bridge (π), and an electron acceptor (A), and they also have one or two anchoring groups to be adsorbed onto the TiO$_2$ surface. In these organic photosensitizers, the movements of electrons are due to intramolecular charge transfer (ICT).[24−26] Organic dyes are usually composed of an electron donor (D), π-conjugated bridges (π), and an electron acceptor (A). The photoabsorption properties of a D−π−A organic dye are associated with the intramolecular charge transfer (ICT) excitation from the donor to the acceptor moiety of the dye, resulting in efficient electron transfer through the acceptor moiety from the excited dye into the TiO$_2$ conduction band. The photo-induced electron transfer from D−π−A organic dyes to TiO$_2$ photoelectrodes can thus efficiently occur by ICT with respect to the HOMO-to-LUMO transition.

In this study, we fabricated three types of TiO$_2$ photoelectrodes to confirm the structure of the TiO$_2$ photoelectrode suitable for the synthesized organic photosensitizers. The relationship of photovoltaic effects and interfacial resistance characteristics of DSSCs using the three organic photosensitizers adsorbed onto the three different TiO$_2$ photoelectrodes could be interpreted from interfacial resistances according to frequency through impedance analysis.

■ RESULTS AND DISCUSSION

The TiO$_2$ photoelectrode of the DSSC mainly has a nanoporous or mesoporous structure. The photosensitizers adsorbed onto the surface of the porous TiO$_2$ photoelectrode generate electrons by separating the photons (electron−hole pair) absorbed from light energy. Therefore, to adsorb a lot of photosensitizers onto the TiO$_2$ photoelectrode, the porous TiO$_2$ photoelectrode should be crystallographically nanoporous and have a large specific surface area. To confirm the crystalline structure of the fabricated three types of TiO$_2$ photoelectrodes (SP type, D type, and SPD type), X-ray diffraction for the three types of TiO$_2$ photoelectrodes was performed.

X-ray diffraction patterns of the three types of TiO$_2$ photoelectrodes in anatase phases are shown in Figure S1. Figure S1 shows that X-ray diffraction patterns of all types of TiO$_2$ photoelectrodes exhibited strong diffraction peaks at 25° and 48° which indicate TiO$_2$ in the anatase phase. All diffraction peaks from lattice planes (101), (004), (200), (105), (211), (204), (116), (220), and (215) confirmed the anatase phase (JCPDS no. 21-1272). Similar patterns could be identified, regardless of the types of TiO$_2$ photoelectrodes with no traceable impurity peaks.

BET analysis shows the three types of TiO$_2$ photoelectrodes after calcination at a temperature of 500 °C in Table 3, and the pore size distribution curves are shown in Figure S2. The specific surface area of the TiO$_2$ photoelectrode in DSSCs greatly affects the amount of photosensitizer adsorption, which plays an important role in total light absorption. As shown in Table 1, the specific surface area values of the TiO$_2$

Table 1. BET Data of SP Type, D Type, and SPD Type TiO$_2$

	SP type TiO$_2$	D type TiO$_2$	SPD type TiO$_2$
BET surface area (m^2/g)	359.98	403.47	442.92
pore volume (cm^3/g)	0.5074	0.4483	0.4333
pore diameter (nm)	28.732	28.233	26.225

photoelectrode are measured at 359.98, 403.47, and 442.92 m^2/g for SP type, D type, and SPD type, respectively. Among the three different types of TiO$_2$ photoelectrodes, the highest specific surface area was obtained in the SPD type. A sufficiently large specific surface area can adsorb large amounts of photosensitizers, which is advantageous for increasing light absorption and photocurrent.

Porosity is another factor that should be optimized to improve the photovoltaic performance on DSSC devices. For fast regeneration of the oxidized dye and charge transportation, the redox electrolyte must be able to penetrate the pores efficiently and be present in places where photosensitizers penetrate. In general, the larger the particle size, the larger the porosity of the layer. When different TiO$_2$ pastes were used to prepare the nanostructured TiO$_2$ photoelectrode, their average pore volumes were measured to be 0.5074, 0.4383, and 0.4333 m^3/g for SP type, D type, and SPD type, respectively. Table 1 shows that the corresponding pore diameters were 28.732 nm, 28.233 nm, and 26.225 nm, respectively. These pore volumes were enough to allow the transportation of iodide/tri-iodide ionic species (I$^-$/I$_3^-$) within the pores of the TiO$_2$ photoelectrodes.

The morphological characteristics and thickness of the TiO$_2$ photoelectrodes were studied by FESEM analysis. In the FE-SEM surface images of TiO$_2$ photoelectrodes on FTO substrates of Figure S3, small grains with dense structures and complete surface coverage were observed. The SP type TiO$_2$ photoelectrodes showed transparent characteristics; however, the D type and SPD type TiO$_2$ photoelectrodes were translucent. The thicknesses of TiO$_2$ photoelectrodes calculated from the cross sections of TiO$_2$ photoelectrodes were about 10 μm (SP type and D type) and 20 μm (SPD type). The formation of densely and uniformly formed thin layers probably could be due to the small TiO$_2$ particles. The SPD type TiO$_2$ photoelectrodes showed small aggregates and relatively complete surface coverage. It can be sufficient for the effect of light scattering to be observed in the double-layered TiO$_2$ photoelectrodes. The formation of a dense bottom layer
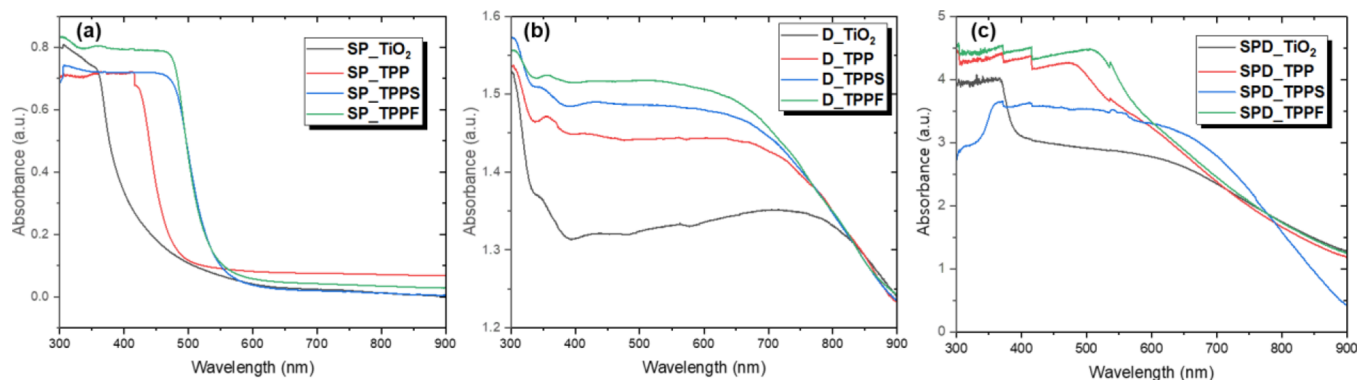
Figure 3. UV−vis absorption spectra of the TPP, TPPS, and TPPF photosensitizers in CHCl₃ (0.5 mM), (a) anchored onto the SP type TiO₂ photoelectrodes, (b) anchored onto the D type TiO₂ photoelectrodes, and (c) anchored onto the SPD type TiO₂ photoelectrodes.
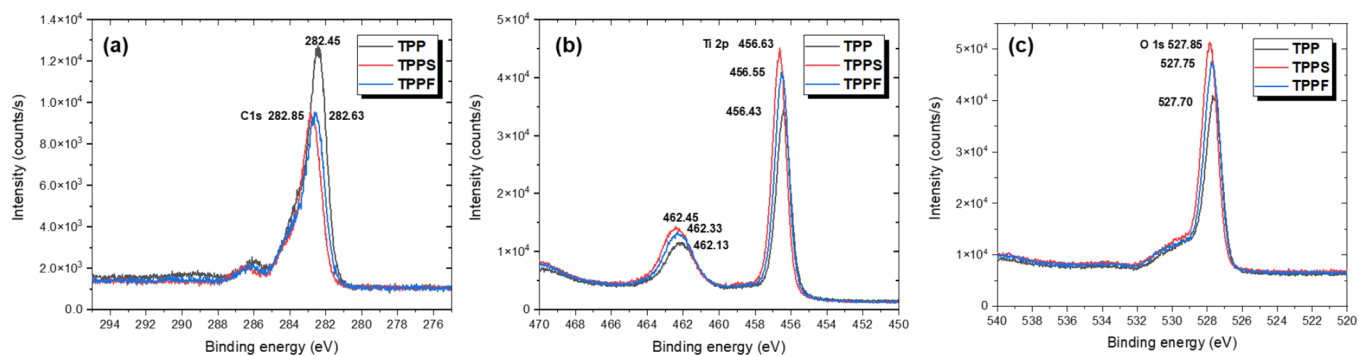
Figure 4. XPS spectra of TPP, TPPS, and TPPF adsorbed onto the SPD type TiO₂; (a) C 1s; (b) Ti 2p; and (c) O 1s.

and a porous top layer was observed in the SPD type TiO₂ photoelectrodes. The compromise between the pore size and the surface area brings sufficient space for the diffusion of the iodide/tri-iodide ionic species into the TiO₂ matrix, leading to maximum conversion efficiency.

The UV−vis absorption spectra of the three photosensitizers (TPP, TPPS, and TPPF) in 0.5 mM CHCl₃ solution and adsorbed onto the three types of TiO₂ photoelectrodes (SP type, D type, and SPD type) are shown in Figure 3. In the CHCl₃ solution, the TPP, TPPS, and TPPF photosensitizers showed two distinct absorption peaks of 338/396, 350/398, and 358/396 nm and maximum absorption wavelengths (λ_{max}) of 338, 350, and 358 nm, respectively.[20] These λ_{max} values correspond to the ICT between the triphenylamine donating unit and the cyanoacrylic acid anchoring moiety. This result shows that the red shift of the λ_{max} is due to the expansion of π-electron conjugation caused by the introduction of thiophene as π-conjugated bridges.

When TPP, TPPS, and TPPF photosensitizers were adsorbed on the TiO₂ surface (SP type), their absorption maxima were 416, 463, and 466 nm, respectively. Their absorption maxima were red-shifted by 78, 113, and 108 nm in comparison to those in the CHCl₃ solution, respectively, due to the interaction of the anchoring group with the surface titanium oxide anions[27] and partial formation of J-type aggregates.[28,29] Among the organic photosensitizers with a bulky structure, there are compounds with a large red-shifted absorption depending on the arrangement of structures. In this study, when three photosensitizers (TPP, TPPS, and TPPF) were adsorbed on the TiO₂ photoelectrode, their arrangement changed to J-type aggregation form, and the absorption peaks were super-largely red-shifted.[30]

Moreover, when TPP, TPPS, and TPPF photosensitizers were adsorbed on the TiO₂ surface (D type and SPD type), their absorptions broadened to over 800 nm in the visible wavelength due to the predominating light scattering effects of D type and SPD type having translucent characteristics. The absorbance remarkably improved the absorption in the range from visible to near IR because of light scattering by additional scattering layers comprising larger nanoparticles. The addition of a light scattering layer in TiO₂ photoelectrodes is adopted as a strategy to improve the light-harvesting ability, and thereby, the interaction of light with the anchored photosensitizers could be enhanced.

The chemical states of the SPD type TiO₂ photoelectrode-anchoring photosensitizers (TPP, TPPS, and TPPF) were investigated by XPS analysis. In Figure 4, characteristic XPS peaks of Ti 2p, C 1s, and O 1s can be observed from the XPS survey spectrum. Their corresponding data are summarized in Table 2. In Figure 4a, C 1s spectra of SPD TiO₂ anchoring organic photosensitizers reveal that only a trace level of C is present in the sample, which also reveals that the carboxylic group takes part only as a structure-directing agent in the formation of organic photosensitizers onto the surface of SPD type TiO₂. In Figure 4b, the XPS spectrum of the Ti 2p shows two distinguishable binding energy peaks at 456.43 and 462.13 eV (for TPP) corresponding to Ti $2p_{3/2}$ and Ti $2p_{1/2}$, respectively, which can be assigned to spin orbitals of Ti⁴⁺ states. Figure 4c shows the deconvoluted O 1s spectrum where the main peak at 527.70 eV (for TPP) is attributed to the TiO₂ crystal lattice, and the small shoulder peak at 531.00 eV (for TPP) can be ascribed to the physically captivated oxygen.[31]

The incident monochromatic photon-to-current conversion efficiency (IPCE) spectra of the DSSC devices based on TPP,

Table 2. XPS Data of TPP, TPPS, and TPPF Adsorbed onto the SPD TypeTiO$_2$

		binding energy (eV)	atomic concentration (%)	mass concentration (%)
SPD_TPP	C 1s	282.45	46.8	29.7
	Ti 2p	456.43	15.0	37.9
	O 1s	527.70	38.2	32.3
SPD_TPPS	C 1s	282.85	33.7	19.2
	Ti 2p	456.63	20.1	45.7
	O 1s	527.85	46.2	35.1
SPD_TPPF	C 1s	282.63	36.9	21.6
	Ti 2p	456.55	18.8	43.8
	O 1s	527.75	44.4	34.6

TPPS, and TPPF photosensitizers as the three types of TiO$_2$ photoelectrodes are presented in Figure 6. The IPCE is defined as the number of electrons that flow through the external circuit divided by the number of incident photons and is calculated using the following equation.

$$IPCE = \{(1240 \times J_{sc})/(\lambda \times P_{in})\} \times 100 \quad (1)$$

where J_{sc} (mA/cm^2) is the short-circuit current density, λ (nm) is the excitation wavelength, and P_{in} (mW/cm^2) is the incident light intensity. Figure 5 shows that TPP, TPPS, and TPPF photosensitizers can efficiently convert visible light to photocurrent in the range between 300 and 600 nm, and the corresponding data are summarized in Table 3. The DSSCs based on TPP, TPPS, and TPPF photosensitizers absorbed onto the three types of TiO$_2$ photoelectrodes produced maximum IPCE values of 31.50~38.19% at 410~430 nm, 26.00~34.74% at 420~450 nm, and 34.79~47.80% at 440~460 nm, respectively. These results show that the red-shift of the maximum IPCE is due to the expansion of π-electron conjugation, which is consistent with the absorption spectra of three organic photosensitizers. All the three organic photosensitizers showed low IPCE results when adsorbed on the D type TiO$_2$ photoelectrode. From these results, it could be predicted that the photovoltaic performances of DSSCs based on D type TiO$_2$ photoelectrodes will be degraded.

The power conversion efficiency of the device was obtained from the performance parameters, open-circuit voltage (V_{oc}), short-circuit current density (J_{sc}), and fill factor (FF). P_{in} and P_{max} represented the incident light power (100 mW/cm^2) and

the maximum power point, respectively. The fill factor was calculated from V_{oc}, J_{sc}, and P_{max} according to the following equations.

Power Conversion Efficiency (η) = P_{max}/P_{in}

$$= (I_{max} \times V_{max})/P_{in} = FF \times \{(I_{sc} \times V_{oc})/P_{in}\} \quad (2)$$

Fill Factor (FF) = $(I_{max} \times V_{max})/(I_{sc} \times V_{oc})$

$$= P_{max}/(I_{sc} \times V_{oc}) \quad (3)$$

Figure 6 shows the $J-V$ curves of the DSSC devices based on TPP, TPPS, and TPPF photosensitizers as the three types of TiO$_2$ photoelectrodes. Cells with an active area of 0.40 cm^2 were fabricated. Nine kinds of DSSC devices were fabricated with three different photosensitizers (TPP, TPPS, and TPPF) and three types of TiO$_2$ photoelectrodes (SP type, D type, and SPD type). The values of J_{sc}, V_{oc}, FF, and η of the DSSC devices under the light intensity of 100 mW/cm^2 at AM 1.5 are listed in Table 3. As shown in Figure 6 and Table 3, the SPD_TPPF-sensitized cell showed the highest η of 2.64% (J_{sc}: 5.69 mA/cm^2, V_{oc}: 0.69 V, FF: 0.67) and the D_TPPS-sensitized cell showed the lowest η of 0.90% (J_{sc}: 2.63 mA/cm^2, V_{oc}: 0.60 V, FF: 0.57) among the nine DSSC devices. The J_{sc} of the DSSCs as TiO$_2$ photoelectrodes, the SPD type (3.84~5.69 mA/cm^2) and SP type (3.24~5.85 mA/cm^2) showed similar results, but D type (2.63~3.69 mA/cm^2) showed significantly lower results. These results showed a similar trend in the surface resistivity (ρ_s) results of TiO$_2$ photoelectrodes. Surface resistivity data of the three types of TiO$_2$ photoelectrodes by 4-probe methods are summarized in Table S1. All samples were measured three times, and their average values were used. The FTO glass was measured in a bare state to compare with TiO$_2$ photoelectrodes. The increase of surface resistivity of the TiO$_2$ photoelectrode can explain the limitation of charge transfer of the TiO$_2$ photoelectrode, and the higher surface resistance (20.96 Ω/square) of the D-type TiO$_2$ photoelectrode predicts that the charge transfer is difficult compared to SPD type or SP type TiO$_2$ photoelectrodes. These results affected the J_{sc} values after the fabrication of DSSC devices. With TiO$_2$ photoelectrodes, the power conversion efficiencies of the DSSCs are in the order of SPD type (1.31~2.64%) > SP type (1.31~2.50%) > D type (0.90~1.54%).

With organic photosensitizers, the power conversion efficiencies of the DSSCs are in the order of TPPF (1.54~2.64%) > TPP (1.24~1.80%) > TPPS (0.90~1.31%).
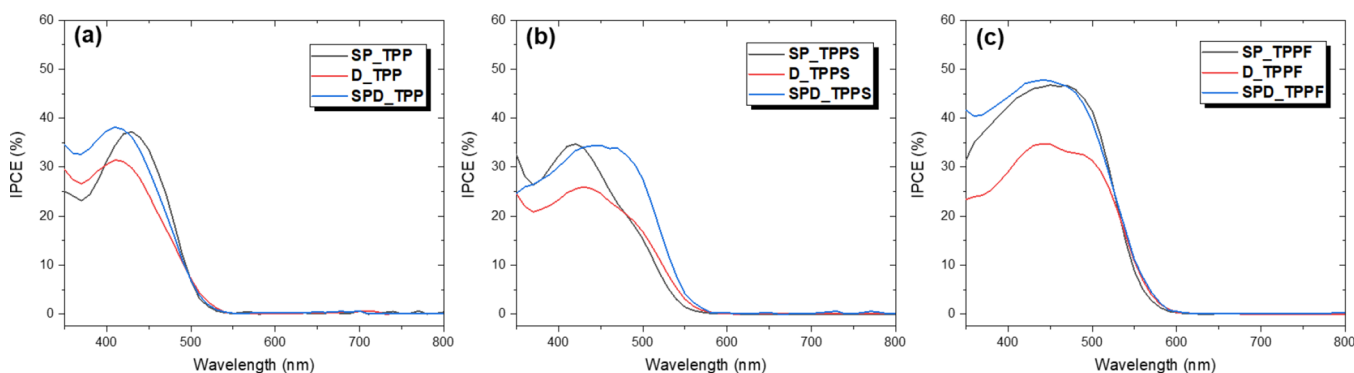
Figure 5. IPCE spectra of DSSC devices based on organic photosensitizers adsorbed onto three types of TiO$_2$ photoelectrodes: (a) TPP, (b) TPPS, and (c)TPPF.

Table 3. Maximum IPCE Data and Photovoltaic Performances of DSSC Devices Based on TPP, TPPS, and TPPF Photosensitizers as the Three Types of TiO$_2$ Photoelectrodes

	maximum IPCE (%)	wavelength (nm)	V_{oc} (V)	J_{sc} (mA/cm^2)	fill factor	efficiency (%)
SP_TPP	37.25	430	0.68	3.24	0.68	1.49
D_TPP	31.50	410	0.69	2.86	0.62	1.24
SPD_TPP	38.19	410	0.72	3.84	0.65	1.80
SP_TPPS	34.74	420	0.61	4.48	0.48	1.31
D_TPPS	26.00	430	0.60	2.63	0.57	0.90
SPD_TPPS	34.48	450	0.59	4.01	0.55	1.31
SP_TPPF	47.10	460	0.66	5.85	0.65	2.50
D_TPPF	34.79	440	0.66	3.69	0.63	1.54
SPD_TPPF	47.80	440	0.69	5.69	0.67	2.64
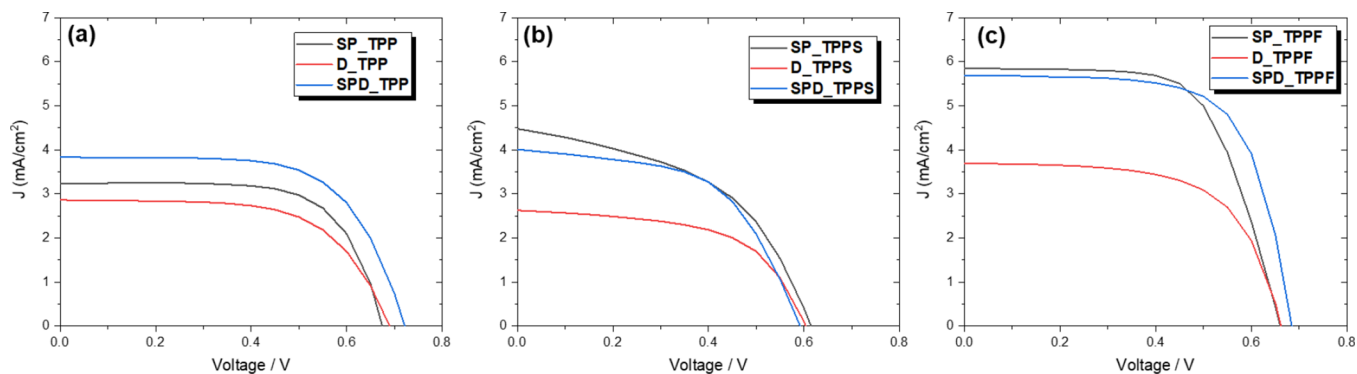
Figure 6. $J-V$ curves of the DSSC devices based on organic photosensitizers adsorbed onto the three types of TiO$_2$ photoelectrodes: (a) TPP, (b) TPPS, and (c)TPPF.

The efficiency results of DSSCs using organic photosensitizers and single- or double-layered TiO$_2$ photoelectrodes in this study were generally lower than those currently reported.[17−19] It was confirmed that the interfacial charge resistance, which acts as an important limiting variable for efficient DSSCs, occurred at the interface organic photosensitizers/TiO$_2$ photoelectrodes, and these DSSCs showed low charge transport at the interface. Therefore, high recombination at the interface resulted in low overall efficiency of DSSCs.

As inferred from the IPCE spectra in Figure 5, the J_{sc} (SP type: 3.24∼5.85 mA/cm^2, D type: 2.63∼2.86 mA/cm^2, and SPD type: 3.84∼5.69 mA/cm^2) of the DSSC devices are shown greatly to be the lower values in the D type TiO$_2$ photoelectrode than those of the other two different types, at all the three photosensitizers as shown in Figure 6. In addition, J_{sc} may be influenced by the amounts of photosensitizers adsorbed on the TiO$_2$ photoelectrode. The amounts of TPP, TPPS, and TPPF adsorbed on the SP type TiO$_2$ photoelectrode were 0.56, 0.43, and 0.90 mmol/cm^3, D type TiO$_2$ photoelectrode were 0.55, 0.40, and 0.80 mmol/cm^3, and the SPD type TiO$_2$ photoelectrode were 0.58, 0.46, and 0.98 mmol/cm^3, respectively. The amounts of photosensitizers adsorbed on the TiO$_2$ photoelectrode were estimated by desorbing photosensitizers in a 50 mM NaOH solution. The D type TiO$_2$ photoelectrode showed a low J_{sc} value due to low light absorption due to low adsorption amounts despite a higher specific surface area than SP type and same TiO$_2$ thickness as SP type. From BET results in Table 1, the specific surface area values of the TiO$_2$ photoelectrode are confirmed at 359.98, 403.47, and 442.92 m^2/g for SP type, D type, and SPD type, respectively. The adsorption amounts and the remaining uncoated TiO$_2$ areas affected not only the J_{sc} but

also the V_{oc}. These results had a great effect on the overall photoconversion efficiency of DSSC devices.

Many factors influence the V_{oc} of the DSSC devices.[32] In general, the V_{oc} of DSSC devices are influenced by the band gap (HOMO/LUMO level) of the photosensitizers. In the previous study, the theoretical band gaps of TPP, TPPS, and TPPF were obtained by the density functional theory (DFT) calculations, and the values were 2.73, 2.43, and 2.44 eV, respectively.[23] Optical band gaps of TPP, TPPS, and TPPF were measured by cyclic voltammetry analysis, and their values were 2.69, 2.36, and 2.38 eV, respectively.[23] The V_{oc} values of TPP (0.68∼0.72 V) were higher than those of TPPS (0.59∼0.61 V) photosensitizers due to their greater band gaps. However, in the case of TPPS (theoretical: 2.43 eV, measured: 2.36 eV) and TPPF (theoretical: 2.44 eV, measured: 2.38 eV) on almost the same bandgap, the V_{oc} values of TPPF (0.66∼0.69 V) were higher than those of TPPS (0.59∼0.61 V), resulting from the Fermi level of the TiO$_2$ photoelectrode and the HOMO level of the coated photosensitizers. In addition, V_{oc} may be influenced by the uncovered TiO$_2$ surface area obtained from the amounts of photosensitizers adsorbed on the TiO$_2$ photoelectrode. This increase in the uncovered TiO$_2$ areas improves the possibility of the redox species accessing the TiO$_2$ surface, allowing electron recombination with the I$_3^-$ acceptor species at the TiO$_2$ surface.

The R_S, $R1_{CT}$, and $R2_{CT}$ are the series resistance, charge transfer resistance of the Pt/electrolyte interface, and charge transfer resistance of the TiO$_2$/photosensitizer/electrolyte interface, respectively.[33] The R_S, $R1_{CT}$, and $R2_{CT}$ values of DSSC devices based on the three photosensitizers (TPP, TPPS, and TPPF) adsorbed onto the three types of TiO$_2$ photoelectrodes are summarized in Table 4. Nyquist plots and

Table 4. Series Resistances (R_S), Charge Transfer Resistances of the Pt/Electrolyte ($R1_{CT}$), TiO$_2$/Photosensitizer/Electrolyte ($R2_{CT}$), and Electron Lifetime of DSSC Devices Using TPP, TPPS, and TPPF Photosensitizers Adsorbed onto the Three Types of TiO$_2$ Photoelectrodes

	SP_TPP	D_TPP	SPD_TPP	SP_TPPS	D_TPPS	SPD_TPPS	SP_TPPF	D_TPPF	SPD_TPPF
Rs (Ω)[a]	15.74	19.52	13.62	20.50	19.82	14.36	14.66	14.10	12.58
$R1_{CT}$ (Ω)[b]	2.76	2.17	2.08	4.20	4.45	5.56	2.07	2.75	2.53
$R2_{CT}$ (Ω)[c]	4.60	4.82	5.90	14.49	21.74	22.56	6.19	6.74	6.73
τ_e (μs)[d]	41.71	32.44	25.24	107.81	152.23	136.22	34.32	32.44	53.61

[a]The series resistance of the DSSC devices. [b]The charge transfer resistance of the Pt/Electrolyte interface. [c]The charge transfer resistance of the TiO$_2$/photosensitizer/electrolyte interface. [d]The electron lifetime (τ_e) of the injected electrons in the TiO$_2$ films determining the frequency f of the middle frequency peak using the equation, $\tau_e = 1/(2\pi f_{peak})$.[33]
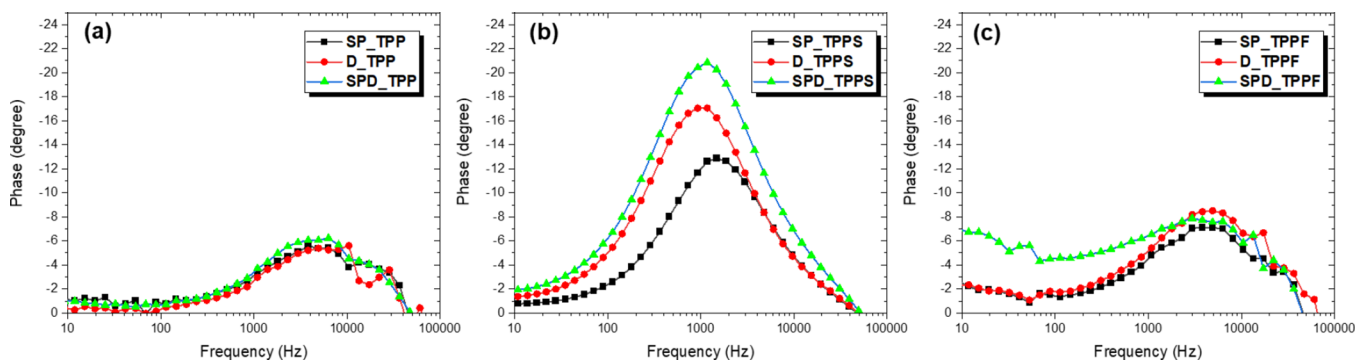
Figure 7. Bode plots of the DSSC device based on organic photosensitizers adsorbed onto the three types of TiO$_2$ photoelectrodes: (a) TPP, (b) TPPS, and (c) TPPF.
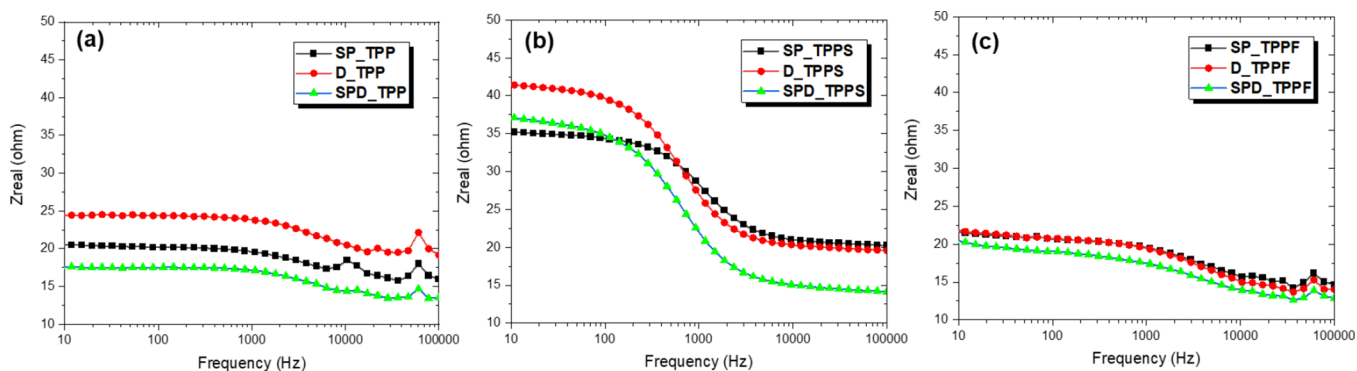
Figure 8. Real part of impedance spectra vs frequency measured in open-circuit conditions for DSSC devices based on organic photosensitizers adsorbed onto the three types of TiO$_2$ photoelectrodes; (a) TPP, (b) TPPS, and (c) TPPF.

Table 5. Real Part of Impedance, Peak Frequency, and Relaxation Time of DSSC Devices Using TPP, TPPS, and TPPF Photosensitizers Adsorbed onto the Three Types of TiO$_2$ Photoelectrodes

	SP_TPP	D_TPP	SPD_TPP	SP_TPPS	D_TPPS	SPD_TPPS	SP_TPPF	D_TPPF	SPD_TPPF
Z_{real} (ohm)[a]	20.50	24.43	17.61	35.20	41.42	37.07	21.61	21.87	20.55
Z_{real} (ohm)[b]	15.99	19.17	13.51	20.25	19.58	14.17	14.66	14.03	12.89
f_{max} (Hz)	3818	3208	3818	1169	579	731	2950	1970	2980
relaxation time (τ, μs)	41.71	49.64	41.71	136.22	275.02	217.83	53.98	80.83	53.43

[a]Real part of impedance at 10 Hz of frequency [b]Real part of impedance at 100,000 Hz of frequency

Bodes plots of DSSC devices are shown in Figure S4 and Figure 7, respectively. The equivalent circuit is shown in Figure S5. The $R1_{CT}$ values of the DSSC devices using three photosensitizers were almost the same regardless of the types of TiO$_2$ photoelectrodes. However, the $R2_{CT}$ values of the DSSC devices based on the three photosensitizers adsorbed onto the three types of TiO$_2$ photoelectrodes are in the order of TPPS (14.49∼22.56 Ω) > TPPF (6.19∼6.74 Ω) > TPP (4.60∼5.90 Ω). DSSC devices using TPPS showed higher

$R2_{CT}$ values, compared to other organic photosensitizers, and these results show a similar tendency in the V_{oc} values of DSSC devices.

Electron lifetime (τ_e) values derived from peak frequency (f_{peak}) in the frequency region corresponding to the TiO$_2$/photosensitizer/electrolyte interface are shown in the Bode plot (Figure 7), according to $\tau_e = 1/2\pi f_{peak}$.[33] Electron lifetime values of TPP, TPPS, and TPPF are listed in Table 4. A longer electron lifetime indicates a more effective suppression of the
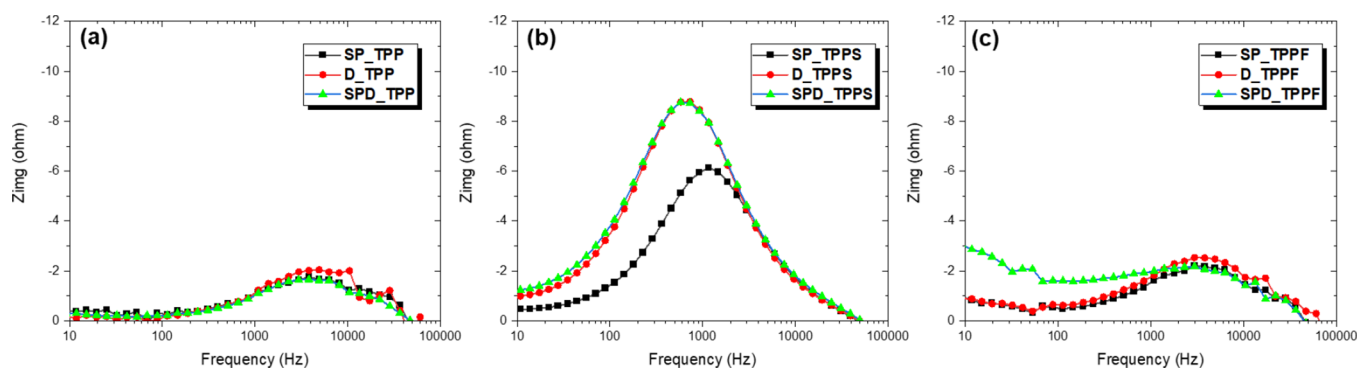
Figure 9. Imaginary part of impedance spectra vs frequency measured in open-circuit conditions for DSSC devices based on organic photosensitizers adsorbed onto the three types of TiO$_2$ photoelectrodes; (a) TPP, (b) TPPS, and (c) TPPF.

back recombination reaction of the injected electrons with I$_3^-$ in the electrolyte.[34] However, the electron lifetime values of these synthesized TPP, TPPS, and TPPF photosensitizers were too low to be considered to affect the performances of DSSC devices.

To further investigate electrical dynamics on DSSCs based on the three photosensitizers (TPP, TPPS, and TPPF) adsorbed onto the three types of TiO$_2$ photoelectrodes, the variation of the real part of impedance (Z_{real}) with frequency is shown in Figure 8. It provides important characteristics of the TiO$_2$ photoelectrodes adsorbed on the photosensitizers, such as (i) the appearance of the peak point at a certain frequency of the spectrum and (ii) coinciding the imaginary part of impedance curves with each other at high frequency. In Figure 8, Z_{real} is plotted as a function of frequency from 10 to 1×10^5 Hz, and the corresponding data are listed in Table 5. At a low frequency of 10 Hz, the values of Z_{real} were 17.61~24.43 Ω for TPP, 35.20~41.42 Ω for TPPS, and 20.55~21.87 Ω for TPPF. The Z_{real} for D type TiO$_2$ photoelectrodes showed higher values, regardless of photosensitizers, showing the highest Z_{real} value in D_TPPS (41.42 Ω). The value of Z_{real} shows a frequency-independent behavior in the low-frequency region. It was observed to gradually decrease as the frequency increased. This phenomenon occurs because the interfacial charge carriers at low frequencies are trapped at the boundary of the TiO$_2$ photoelectrode-adsorbed photosensitizers and can be easily relaxed when an electric field is applied. In addition, this can lead to an excess of the capacitance depending on the time constant and frequency of the interfacial states, thus contributing to the conduction of the TiO$_2$ photoelectrode-adsorbed photosensitizers. At the middle frequency (1000~10,000 Hz), the value of Z_{real} depends on the frequency. It can be confirmed that the conductivity of the TiO$_2$ photoelectrode-adsorbed photosensitizers increases as the frequency increases. Finally, at a higher frequency, all values of Z_{real} are very low and space charge polarization can appear at the interface of the TiO$_2$ photoelectrode-adsorbed photosensitizers due to the reduced barrier properties of TiO$_2$. The presence of space charge polarization in the sample is predicted based on the high Z_{real} values observed at lower frequencies.[35,36] Moreover, at higher frequencies (over 10,000 Hz), the values of Z_{real} are found to be frequency-independent, suggesting the release of space charge.[37,38] The space charge (or interfacial) polarization occurs when there is an accumulation of charge at the interface between two materials (TiO$_2$ photoelectrodes adsorbed the photosensitizers/electrolyte) or between two regions (TiO$_2$ photoelectrode/photo-

sensitizer) within a material (TiO$_2$ photoelectrodes adsorbed the photosensitizer) because of an external field. This can occur when there is a compound dielectric or when there are two electrodes connected to a dielectric material. From these results, it was confirmed that the poor interfacial contact in the D type TiO$_2$ photoelectrode caused an increase in the interfacial charge-transfer resistance between TiO$_2$ photo-electrode-adsorbed photosensitizers and the electrolyte in the DSSC system, and this resulted in degrading J_{sc} and power conversion efficiency. In the case of the SPD type TiO$_2$ photoelectrode, at 100,000 Hz frequency, the values of Z_{real} were 13.51~19.71 Ω for TPP, 14.17~20.25 Ω for TPPS, and 12.89~14.66 Ω for TPPF. The good interfacial contact in the SPD type TiO$_2$ photoelectrode improved the J_{sc}, FF, and power conversion efficiency.

The variation of the imaginary part of impedance (Z_{img}) as a function of frequency is shown in Figure 9. This behavior shows the presence of space charge polarization in the system.[35-37] The values of Z_{img} increase as the frequency increases and reach a peak maximum at a peculiar frequency. Then, the Z_{img} gradually drops off as the frequency continues to increase. It can be seen that the region to the left of the peak maxima value represents the long-range movement of charge carriers and the region to the right represents the localized movement of charge carriers. The frequency at which Z_{img} attains a maximum value is the relaxation frequency (f_{max}). The relaxation time (τ) can then be calculated using the relation: $\tau = 1/2\pi f_{max}$. Thus, the Z_{img} spectra with frequency exhibit the asymmetrical pattern of the peak, a reduction in the height of the peak with a reduction of resistance, and a shifting of the peak toward the high frequency side with a reduction of resistance. The asymmetry broadening of the peak provides an idea about the spread of relaxation time. The peak heights in the Z_{img} spectra are strongly related to bulk resistance (R_b). It can be calculated by the equation $Z_{img} = R_b\{f*\tau/1 + f^2\tau^2\}$. The shifting of the peak toward high frequency causes the reduction of bulk resistance of the material. In Figure 9 and Table 5, the peak frequencies of TPP, TPPS, and TPPF were 3208~3818 Hz, 1169~579 Hz, and 1970~2980 Hz, respectively. The relaxation times of TPP, TPPS, and TPPF were calculated as 41.71~49.64 μs, 136.22~275.02 μs, and 53.43~80.83 μs, respectively. In particular, when the D type TiO$_2$ photo-electrode was applied to the same photosensitizer, the maximum peak was shifted toward a low frequency, that is, to the left. As a result, it was found that the resistance increased when using the D type TiO$_2$ photoelectrode, which affected the J_{sc} and photoconversion efficiency. Also, in Figure 9, the

dispersion of Z_{img} spectra in the low frequency and their merging at high frequency exhibited the disappearance of space charge polarization at high frequency.[38]

CONCLUSIONS

We fabricated three different types of TiO_2 photoelectrodes (SP type, D type, and SPD type) to obtain excellent performances of the DSSCs using optimal TiO_2 photo-electrodes for the synthesized pyrazine-based organic photo-sensitizers (TPP, TPPS, and TPPF) and evaluated the performance of DSSCs. Double-layered (SPD type) and single-layered (SP type and D type) TiO_2 photoelectrodes prepared from different pastes showed the same crystal structure, and moreover, their values of specific surface area, pore volume, and pore diameter did not show significant differences. The DSSC device using double-layered SPD type TiO_2 photoelectrodes displayed 1.31∼2.64% efficiency, compared to single-layered SP type (1.31∼2.50%) and single-layered D type (0.90∼1.54%), using organic photo-sensitizers. The DSSC device using double-layered SPD type TiO_2 photoelectrode and TPPF as a photosensitizer (SPD_TPPF) showed the highest J_{sc} of 5.69 mA/cm², V_{oc} of 0.69 V, FF of 0.67, and efficiency of 2.64%. However, the photovoltaic characteristics of D type TiO_2 photoelectrodes were peculiarly lower than those of other TiO_2 photo-electrodes. Despite having the same crystal structure and similar specific surface area, pore volume, and pore diameter, the D type TiO_2 photoelectrode with low IPCE and low adsorption amount led to a decrease in photocurrent density. To elucidate these results, we evaluated the interfacial resistance characteristics using EIS analysis. Through Z_{real} and Z_{img}, it was confirmed that the interfacial resistance was large in the D type TiO_2 photoelectrode, and this affected on the current density and FF, and thus, the photovoltaic performances of DSSC devices were reduced.

EXPERIMENTAL SECTION

Materials and Regents. Fluorine-doped SnO_2 glass (FTO glass, sheet resistance 15 Ω/square) was purchased from Solaronix SA (Aubonne, Switzerland). Ti-Nanoxide BL/SP (compact TiO_2 paste), Ti-Nanoxide T/SP (transparent TiO_2 paste), Ti-Nanoxide D/SP (dispersed TiO_2 paste), Iodolyte HI-30, N719 dye, and Surlyn (SX1170-25) were purchased from Solaronix SA (Aubonne, Switzerland). All reagents and solvents were obtained from Aldrich and TCI (South Korea). They were of analytical grade and used as received without further purification.

Measurements. UV−vis absorption and fluorescence emission spectra were obtained on a V-730 UV−visible spectrophotometer (Jasco, TS Science Co., Ltd., Seoul, South Korea) at ambient temperature. Morphologies and thicknesses of nanoporous TiO_2 layers were observed by FE-SEM (TESCAN, MIRA 3 LMH In-Beam Detector) (TESCAN Korea, Seoul, South Korea). The BET method was used to observe the nanoporous TiO_2 layers using the surface area and pore size analyzer (Quantachrome (Autosorb-iQ)). XRD analysis was conducted on a X'Pert3-Powder (PANalytical) at a voltage of 40 kV and a current of 30 mA with Cu-Kα radiation (λ = 1.540 A), employing a scanning step width of 0.026 ° in the range of 20∼80°. An XPS measurement was carried out on an AXIS SUPRA (KRATOS Analytical Ltd.) using a monochromatic Al X-ray source operating at 225 W.

During the XPS measurements, emission lines were calibrated using the C1s signal at 286.69 eV. Irradiated current density−voltage ($J−V$) curves were tested using a Keithley 2400 under air mass 1.5 global (AM 1.5G) irradiation (100 mW/cm²) (Tektronix Korea, Seoul, South Korea). The light intensity was calibrated using an NREL-Si solar cell. External quantum efficiency (EQE) was measured under monochromatic light using a xenon lamp (Dongwoo Optron, Kyeonggido, South Korea). Electrical impedance spectroscopy (EIS) measure-ments were performed using an Ivium compact Stat.h electrochemical analyzer (AR Eindhoven, Netherlands). EIS data were obtained with an impedance analyzer in the frequency range of 0.1∼1 MHz at room temperature using FTO/TiO_2/photosensitizer/electrolyte/Pt/FTO cells. The interfacial charge transfer resistances of DSSC devices based on the three photosensitizers (TPP, TPPS, and TPPF) adsorbed onto the three types of TiO_2 photoelectrodes were calculated using EIS measurements to investigate the effect of the interfacial charge transfer on the photovoltaic perform-ances of the DSSC devices. EIS measurements of DSSC devices were recorded at −0.60 V at a frequency range of 0.1 Hz to 1 MHz in the dark. The applied voltage is equivalent to the approximate V_{oc} of DSSC measured. Surface resistivity (ρ_s) of TiO_2 photoelectrodes was measured using four-probe method by using Loresta-GX with a PSP Probe at room temperature.[39,40] The distance between probes was 2.0 mm and the size of the testing TiO_2 photoelectrodes on the FTO glass was 2.0 mm × 1.5 mm. The constant resistivity correction factor (RCF) of 4.532 was applied. The RCF was used to obtain correct values for surface resistivity.

Fabrications of Mono- or Double-Layered TiO_2 Photoelectrodes. As shown in Figure 2, three types of TiO_2 photoelectrodes onto the FTO glass substrate (15 Ω/ square) were prepared by layer-by-layer deposition of mono- or double-layered TiO_2 pastes by calcinations after coating with the doctor blade method. Formerly, a compact TiO_2 layer (blocking layer) was applied onto the FTO glass substrate to facilitate contact between the FTO glass substrate and TiO_2 layer. The TiO_2 layer was sintered sequentially at 120 °C for 30 min and 500 °C for 30 min. After the sintering process, the TiO_2-deposited electrode was cooled down from 500 °C to room temperature at a controlled cooling rate (5 °C/min) to avoid any cracking of the glass. The double-layered TiO_2 photoelectrode was prepared by repeating squeezing and the following calcination process. SP type and D type composing of homogeneous TiO_2 layers are regarded as a mono-layer, whereas SPD type consisting two different TiO_2 layers is regarded as a double-layer.

Fabrications of DSSC Devices. The working electrode was prepared as follows. Three types of TiO_2 photoelectrodes were fabricated as SP type, D type, and SPD type. The thickness of the TiO_2 photoelectrodes, measured from the FESEM cross-section image, was about 10 μm for SP type, 10 μm for D type, and 20 μm for SPD type. The three types of TiO_2 photoelectrodes were dipped in a 0.5 mM $CHCl_3$ solution of photosensitizers and left to stand for 48 h at room temperature, respectively. Three photosensitizers (TPP, TPPS, and TPPF) were used. Their syntheses and character-istics are described in the previous article.[20] The electrolyte used was Iodolyte HI-30 that consisted of 30 mM iodide/tri-iodide in acetonitrile. Platinum paste was spread on the FTO glass substrate, which had holes for the injection of the electrolytes, and was sintered sequentially at 120 °C for 30 min

and 500 °C for 30 min. After the sintering process, the counter electrode was cooled down from 500 °C to room temperature at a controlled cooling rate (5 °C/min). To assemble the DSSC devices, the working electrode and the counter electrode were attached using a 60 μm-thick Surlyn. The space between the two electrodes was filled with the electrolyte described above. After the injection of the electrolyte, the holes on the counter electrode were sealed using cover glasses to prevent its evaporation. To prevent inflated photocurrents arising from stray light, a black mask surrounded the active area. The active area of the DSSC device was 0.40 cm^2.

■ ASSOCIATED CONTENT

Ⓢ Supporting Information

The Supporting Information is available free of charge at https://pubs.acs.org/doi/10.1021/acsomega.3c00707.

X-ray diffraction, pore size distribution curves, FE-SEM images, Nyquist plots, equivalent circuit, surface resistivity (PDF)

■ AUTHOR INFORMATION

Corresponding Author

Songyi Lee − Department of Chemistry and Industry 4.0 Convergence Bionics Engineering, Pukyong National University, Busan 48513, Korea; ⊙ orcid.org/0000-0002-8788-6056; Email: slee@pknu.ac.kr

Authors

Mi-Ra Kim − Department of Chemistry, Pukyong National University, Busan 48513, Korea

Thanh Chung Pham − Industry 4.0 Convergence Bionics Engineering, Pukyong National University, Busan 48513, Korea; Vietnam Academy of Science and Technology, Institute for Tropical Technology, Hanoi 1000, Vietnam

Hyun-Seock Yang − Department of Physics, Pukyong National University, Busan 48513, Korea

Sung Heum Park − Department of Physics, Pukyong National University, Busan 48513, Korea; ⊙ orcid.org/0000-0001-5701-660X

Seah Yang − Industry 4.0 Convergence Bionics Engineering, Pukyong National University, Busan 48513, Korea

Myeongkee Park − Department of Chemistry, Pukyong National University, Busan 48513, Korea; ⊙ orcid.org/0000-0002-5307-2564

Sang Gil Lee − Department of Food Science and Nutrition, Pukyong National University, Busan 48513, Korea

Complete contact information is available at:
https://pubs.acs.org/10.1021/acsomega.3c00707

Notes

The authors declare no competing financial interest.

■ ACKNOWLEDGMENTS

■ REFERENCES

(1) Feltrin, A.; Freundlich, A. Material considerations for terawatt level deployment of photovoltaics. *Renewable Energy* **2008**, *33*, 180−185.

(2) Tennakone, K.; Kumara, G. R. R. A.; Kottegoda, I. R. M.; Perera, V. P. S. An efficient dye sensitized photoelectrochemical solar cell made from oxides of tin and zinc. *Chem. Commun.* **1999**, 15−16.

(3) Sayama, K.; Sugihara, H.; Arakawa, H. Photoelectrochemical Properties of a Porous Nb2O5 Electrode Sensitized by a Ruthenium Dye. *Chem. Mater.* **1998**, *10*, 3825−3832.

(4) O'Regan, B.; Grätzel, M. A low-cost, high-efficiency solar cell based on dye-sensitized colloidal TiO2 films. *Nature* **1991**, *353*, 737−740.

(5) Hagfeldt, A.; Boschloo, G.; Sun, L.; Kloo, L.; Pettersson, H. Dye-sensitized solar cells. *Chem. Rev.* **2010**, *110*, 6595−6663.

(6) Grätzel, M. Photoelectrochemical cells. *Nature* **2001**, *414*, 338−344.

(7) Grätzel, M. Recent advances in sensitized mesoscopic solar cells. *Acc. Chem. Res.* **2009**, *42*, 1788−1798.

(8) Kalyanasundaram, K. *Dye-sensitized Solar Cells*; CRC; Taylor & Francis: Boca Raton, Fla., London, 2010.

(9) Kavan, L.; Grätzel, M.; Gilbert, S. E.; Klemenz, C.; Scheel, H. J. Electrochemical and photoelectrochemical investigation of single-crystal anatase. *J. Am. Chem. Soc.* **1996**, *118*, 6716−6723.

(10) Carp, O.; Huisman, C. L.; Reller, A. Photoinduced reactivity of titanium dioxide. *Prog. Solid State Chem.* **2004**, *32*, 33−177.

(11) Dambournet, D.; Belharouak, I.; Amine, K. Tailored preparation methods of TiO2 anatase, rutile, brookite: Mechanism of formation and electrochemical properties. *Chem. Mater.* **2010**, *22*, 1173−1179.

(12) Chen, X.; Mao, S. S. Titanium dioxide nanomaterials: synthesis, properties, modifications and applications. *Chem. Rev.* **2007**, *107*, 2891−2959.

(13) Gu, F.; Huang, W.; Wang, S.; Cheng, X.; Hu, Y.; Lee, P. S. Open-circuit voltage improvement in tantalum-doped TiO2 nano-crystals. *Phys. Chem. Chem. Phys.* **2014**, *16*, 25679−25683.

(14) Archana, P. S.; Gupta, A.; Yusoff, M. M.; Jose, R. Tungsten doped titanium dioxide nanowires for high efficiency dye-sensitized solar cells. *Phys. Chem. Chem. Phys.* **2014**, *16*, 7448−7454.

(15) Wu, X.; Jiang, Q. Z.; Ma, Z. F.; Fu, M.; Shangguan, W. F. Synthesis of titania nanotubes by microwave irradiation. *Solid State Commun.* **2005**, *136*, 513−517.

(16) Peng, X.; Chen, A. Aligned TiO2 nanorod arrays synthesized by oxidizing titanium with acetone. *J. Mater. Chem.* **2004**, *14*, 2542−2548.

(17) Zhang, W.; Gu, J.; Yao, S.; Wang, H. The synthesis and application of TiO2 microspheres as scattering layer in dye-sensitized solar cells. *J. Mater. Sci.: Mater. Electron.* **2018**, *29*, 7356−7363.

(18) Chen, Y. Z.; Wu, R. J.; Lin, L. Y.; Chang, W. C. Novel synthesis of popcorn-like TiO2 light scatterers using a facile solution method for efficient dye-sensitized solar cells. *J. Power Sources* **2019**, *413*, 384−390.

(19) Khakpour, Z.; Tavassoli, M.; Moradlou, O. Sol−gel approach for the growth of vertically aligned 3D-TiO2 nanorod arrays as an efficient photoanode for high-performance dye-sensitized solar cells. *J. Iran Chem. Soc.* **2020**, *17*, 881−891.

(20) Areerob, Y.; Hamontree, C.; Sricharoen, P.; Limchoowong, N.; Nijpanich, S.; Nachaithong, T.; Oh, W.-C.; Pattarith, K. Synthesis of novel MoWO4 with ZnO nanoflowers on multi-walled carbon nanotubes for counter electrode application in dye-sensitized solar cells. *Nature* **2022**, *12*, 12490.

(21) Oh, W.-C.; Liu, Y.; Areerob, Y. A novel fabrication of organic-inorganic hybridized Graphene-La2CrFeW6 nanocomposite and its improved photovoltaic performance in DSSCs. *J. Sci.: Adv. Mater. Devices* **2021**, *6*, 271−279.

(22) Choi, J.; Song, S.; Hörantner, M. T.; Snaith, H. J.; Park, T. Well-Defined Nanostructured, Single-Crystalline TiO2 Electron Transport Layer for Efficient Planar Perovskite Solar Cells. *ACS Nano* **2016**, *10*, 6029−6036.

(23) Kim, M.-R.; Pham, T. C.; Choi, Y.; Yang, S.; Yang, H.-S.; Park, S. H.; Kang, M.; Lee, S. Syntheses and Photovoltaic Properties of New Pyrazine-Based Organic Photosensitizers for Dye-Sensitized Solar Cells. *Energies* **2022**, *15*, 5938.

(24) Yu, J.; Shen, T. L.; Weng, W. H.; Huang, Y. C.; Huang, C. I.; Su, W. F.; Rwei, S.-P.; Ho, K.-C.; Wang, L. Molecular design of interfacial modifiers for polymer-inorganic hybrid solar cells. *Adv. Energy Mater.* **2012**, *2*, 245−252.

(25) Xiao, Y.; Su, X.; Lydia, S. V.; Lacaze, E.; Heinrich, B.; Donnio, B.; Kreher, D.; Mathevet, F.; Attias, A.-J. Chemical engineering of donor−acceptor liquid crystalline dyads and triads for the controlled nanostructuration of organic semiconductors. *CrystEngComm* **2016**, *18*, 4787−4798.

(26) Park, H.-H.; Meti, P.; Gong, Y. D. Effect of conjugation on the optoelectronic properties of pyrazine-based push-pull chromophores: Aggregation-induced emission, solvatochromism, and acidochromism. *Dyes Pigm.* **2021**, *190*, No. 109320.

(27) Jung, I.; Lee, J. K.; Song, K. H.; Song, K. H.; Kang, S. O.; Ko, J. J. Synthesis and Photovoltaic Properties of Efficient Organic Dyes Containing the Benzo[b]furan Moiety for Solar Cells. *J. Org. Chem.* **2007**, *72*, 3652−3658.

(28) Sayama, K.; Tsukagoshi, S.; Mori, T.; Hara, K.; Ohga, Y.; Shinpou, A.; Abe, Y.; Suga, S.; Arakawa, H. Efficient sensitization of nanocrystalline TiO2 films with cyanine and merocyanine organic dyes. *Sol. Energy Mater. Sol. Cells* **2003**, *80*, 47−71.

(29) Horiuchi, T.; Miura, H.; Uchida, S. Highly efficient metal-free organic dyes for dye-sensitized solar cells. *J. Photochem. Photobiol., A* **2004**, *164*, 29−32.

(30) Zhao, L.; Ren, X.; Yan, X. Assembly Induced Super-Large Red-Shifted Absorption: The Burgeoning Field of Organic Near-Infrared Materials. *CCS Chem.* **2021**, *3*, 678−693.

(31) Zhao, Z.; Sun, Z.; Zhao, H.; Zheng, M.; Du, P.; Zhao, J.; Fan, H. Phase control of hierarchically structured mesoporous anatase TiO2 microspheres covered with {001} facets. *J. Mater. Chem.* **2012**, *22*, 21965−21971.

(32) Borbon, S.; Lugo, S.; Pourjafari, D.; Aguilar, N. P.; Oskam, G.; López, I. Open-Circuit Voltage (VOC) Enhancement in TiO2-Based DSSCs: Incorporation of ZnO Nanoflowers and Au Nanoparticles. *ACS Omega* **2020**, *5*, 10977−10986.

(33) Kern, R.; Sastrawan, R.; Ferber, J.; Stangl, R.; Luther, J. Modeling and interpretation of electrical impedance spectra of dye solar cells operated under open-circuit conditions. *Electrochim. Acta* **2002**, *47*, 4213−4225.

(34) Kuang, D.; Uchida, S.; Humphry-Baker, R.; Zakeeruddin, S. M.; Grätzel, M. Organic Dye-Sensitized Ionic Liquid Based Solar Cells: Remarkable Enhancement in Performance through Molecular Design of Indoline Sensitizers. *Angew. Chem., Int. Ed.* **2008**, *47*, 1923−1927.

(35) Jonscher, K. The 'universal' dielectric response. *Nature* **1977**, *267*, 673−679.

(36) Singh, B. K.; Kumar, B. Impedance analysis and high temperature conduction mechanism of flux grown Pb(Zn1/3Nb2/3)0.91Ti0.09O3 single crystal. *Cryst. Res. Technol.* **2010**, *45*, 1003−1011.

(37) Maier, J. Defect chemistry and ion transport in nanostructured materials: Part II Aspects of nanoionics. *Solid State Ionics* **2003**, *157*, 327−334.

(38) Sinclair, D. C.; West, A. R. Effect of atmosphere on the PTCR properties of BaTiO3 ceramics. *J. Mater. Sci.* **1994**, *29*, 6061−6068.

(39) Naftaly, M.; Das, S.; Gallop, J.; Pan, K.; Alkhalil, F.; Kariyapperuma, D.; Constant, S.; Ramsdale, C.; Hao, L. Sheet Resistance Measurements of Conductive Thin Films: A Comparison of Techniques. *Electronics* **2021**, *10*, 960.

(40) Ramos, R.; Scoca, D.; Merlo, R. B.; Marques, F. C.; Alvarez, F.; Zagonel, L. F. Study of nitrogen ion doping of titanium dioxide films. *Appl. Surf. Sci.* **2018**, *443*, 619−627.